

Research Articles: Systems/Circuits

Prefrontal cortex driven dopamine signals in the striatum show unique spatial and pharmacological properties

<https://doi.org/10.1523/JNEUROSCI.1327-20.2020>

Cite as: J. Neurosci 2020; 10.1523/JNEUROSCI.1327-20.2020

Received: 27 May 2020

Revised: 22 July 2020

Accepted: 17 August 2020

This Early Release article has been peer-reviewed and accepted, but has not been through the composition and copyediting processes. The final version may differ slightly in style or formatting and will contain links to any extended data.

Alerts: Sign up at www.jneurosci.org/alerts to receive customized email alerts when the fully formatted version of this article is published.

1 **Prefrontal cortex driven dopamine signals in the striatum show unique spatial and**
2 **pharmacological properties**

3

4 Martín F. Adrover^{*.1.#}, Jung Hoon Shin^{*.1}, Cesar Quiroz², Sergi Ferré², Julia C. Lemos^{1.#}, and
5 Veronica A. Alvarez^{1,3}

6

7 1, Laboratory on Neurobiology of Compulsive Behavior, Intramural Research Program, National
8 Institute on Alcohol Abuse and Alcoholism, National Institutes of Health, Bethesda, MD 20892

9 2, Integrative Neurobiology Section, National Institute on Drug Abuse, Intramural Research
10 Program, National Institutes of Health, Baltimore, MD 21224

11 3, Center on Compulsive Behaviors, National Institutes of Health, Bethesda, MD 20892

12

13 * authors contributed equally to the work

14 # current address for MFA is Instituto de Investigaciones en Ingeniería Genética y Biología
15 Molecular (INGEBI), CONICET, Buenos Aires, C1428ADN, Argentina. Current address for
16 JCL is Department of Neuroscience, University of Minnesota, Minneapolis, Minnesota 55455.

17

18 ORCID ID

19 Martín F. Adrover: 0000-0002-5294-739X

20 Jung Hoon Shin: 0000-0002-9892-1275

21 Sergi Ferré: 0000-0002-1747-1779

22 Julia C. Lemos: 0000-0002-5442-8876

23 Veronica A. Alvarez: 0000-0003-2611-8675

24 Correspondence should be addressed to Dr. Veronica A. Alvarez, NIAAA-NIH, 5625 Fishers
25 Lane, Bethesda, MD 20892. Email: alvarezva@mail.nih.gov

26

27 **Abbreviated title:** Prefrontal cortex driven striatal dopamine signals

28

29 **Author contributions:** M.F.A., J.H.S. performed all *in vitro* electrophysiology and voltammetry
30 experiments and analyzed data. C.Q. and S.F. performed *in vivo* microdialysis experiments.
31 J.C.L. performed histological quantification. M.F.A., J.H.S. and V.A.A. designed research and
32 wrote the paper.

33

34

35 **Key words:** fast-scan cyclic voltammetry, DA release, optogenetics, prefrontal cortex,
36 dorsomedial striatum

37 **Number of pages:** 42

38 **Number of figures:** 6

39 **Word count:** Abstract: 248 (250 words maximum, including citations)

40 Significance Statement: 120 (120 words maximum)

41 Introduction: 627 (650 words maximum, including citations)

42 Discussion: 1,499 (1,500 words maximum, including citations)

43

44 **Conflict of interest:** The authors declare no competing financial interests.

45

46 **Acknowledgements:** This study was funded by the Intramural Programs of NIAAA, NINDS
47 (ZIA-AA000421) and NIDA. We are grateful to Roland Bock (NIAAA, NIH) for development
48 of the VIGOR acquisition and analysis software, to Drs. Deisseroth (Stanford University) and
49 Boyden for providing the channelrhodopsin-2 and ChrimsonR constructs, respectively. We also
50 thank the members of the Alvarez lab for their valuable comments on the manuscript. The
51 authors declare no competing financial interests.

52

53

54

55 **Abstract**

56 Dopamine (DA) signals in the striatum are critical for a variety of vital processes, including
57 motivation, motor learning and reinforcement learning. Striatal DA signals can be evoked by
58 direct activation of inputs from midbrain DA neurons (DANs) as well as cortical and thalamic
59 inputs to the striatum. In this study, we show that *in vivo* optogenetic stimulation of prelimbic
60 (PrL) and infralimbic (IL) cortical afferents to the striatum triggers an increase in extracellular
61 DA concentration, which coincides with elevation of striatal acetylcholine (ACh) levels. This
62 increase is blocked by a nicotinic ACh receptor (nAChR) antagonist. Using single or dual
63 optogenetic stimulation in brain slices from male and female mice, we compared the properties
64 of these PrL/IL evoked DA signals with those evoked by stimulation from midbrain DAN axonal
65 projections. PrL/IL evoked DA signals are undistinguishable from DAN evoked DA signals in
66 their amplitudes and electrochemical properties. However, PrL/IL evoked DA signals are
67 spatially restricted and preferentially recorded in the dorsomedial striatum. PrL/IL evoked DA
68 signals also differ in their pharmacological properties, requiring activation of glutamate and
69 nicotinic ACh receptors. Thus, both *in vivo* and *in vitro* results indicate that cortical evoked DA
70 signals rely on recruitment of cholinergic interneurons (CINs), which renders DA signals less
71 able to summate during trains of stimulation and more sensitive to both cholinergic drugs and
72 temperature. In conclusion, cortical and midbrain inputs to the striatum evoke DA signals with
73 unique spatial and pharmacological properties that likely shape their functional roles and
74 behavioral relevance.

75 (248 / 250 words)

76

77

78 **Significance Statement (120 words maximum)**

79 Dopamine signals in the striatum play a critical role in basal ganglia function such as
80 reinforcement and motor learning. Different afferents to the striatum can trigger dopamine
81 signals, but their release properties are not well understood. Further, these input-specific
82 dopamine signals have only been studied in separate animals. Here we show that optogenetic
83 stimulation of cortical glutamatergic afferents to the striatum triggers dopamine signals both *in*
84 *vivo* and *in vitro*. These afferents engage cholinergic interneurons, which drive dopamine release
85 from dopamine neuron axons by activation of nicotinic acetylcholine receptors. We also show
86 that cortically evoked dopamine signals have other unique properties, including spatial restriction
87 and sensitivity to temperature changes than dopamine signals evoked by stimulation of midbrain
88 dopamine neuron axons.

89 (120/120 words)

90

91

92

93 **Introduction (650 words maximum, including citations)**

94 The striatum receives dense innervation from midbrain DANs, which are the main source
95 of DA in the striatum. DA plays a critical neuromodulatory role in regulating striatal circuitry
96 and function (Surmeier et al., 2007; Gerfen and Surmeier, 2011; Burke et al., 2017). Disruptions
97 in striatal DA levels are associated with many neurological and psychiatric disorders, such as
98 Parkinson's disease and substance abuse disorder (Gerfen, 2000; Luscher et al., 2020). DA is
99 released from a fraction of the varicosities distributed along DAN axons, which contain
100 specialized active zone-like sites (Sulzer et al., 2016; Liu et al., 2018; Liu and Kaeser, 2019).
101 The axonal arborizations of DANs ramify extensively within the striatum and a single dopamine
102 axon can spread over a significant area (around 3% in average) of the striatum (Matsuda et al.,
103 2009). DA released from axonal varicosities generates a rapid increase in local extracellular DA
104 concentration. This extracellular increase leads to the activation of multiple types of DA
105 receptors which are localized in dendrites, somas, and presynaptic terminals. Ultimately, this
106 impacts the network activity of the striatum and drives behavior output (Tritsch and Sabatini,
107 2012; Chuhma et al., 2014; Mamaligas et al., 2016; Burke et al., 2017; Shin et al., 2017; Lahiri
108 and Bevan, 2020). This striatal DA signal is known to be triggered by two mechanisms. One
109 mechanism involves action potential firing initiated at midbrain DAN somas, which propagates
110 through dense axonal arborizations to reach active zone-like release sites in the striatum
111 (Matsuda et al., 2009; Liu et al., 2018). In the other mechanism, DAN axons in the striatum are
112 locally activated, independent of the action potential firing at DAN somas. This mode of DA
113 release requires the activation of nAChRs expressed on DAN axons and synchronized activation
114 of CINs, which is thought to give rise to local release of ACh (Cachope et al., 2012; Threlfell et
115 al., 2012; Wang et al., 2014; Shin et al., 2015; Shin et al., 2017).

116 This local intrastriatal trigger of DA release has only recently been demonstrated and is
117 gaining attention as it represents a newly discovered means for striatal DA
118 modulation/transmission. However, little is known about the differential/unique biophysical and
119 pharmacological properties of locally evoked versus DAN-evoked DA transmission. Recent *in*
120 *vitro* studies utilizing optogenetic stimulation and fast-scan cyclic voltammetry (FSCV) show
121 that local DA signals can be triggered in the striatum by stimulation of glutamatergic inputs from
122 thalamus (Threlfell et al., 2012; Kosillo et al., 2016; Johnson et al., 2017; Cover et al., 2019),
123 motor cortex (Kosillo et al., 2016), or prefrontal cortex (PFC) (Mateo et al., 2017). These
124 findings agree with previous literature showing *in vivo* DA signals in the striatum evoked by
125 stimulation of PFC (Taber and Fibiger, 1993; Quiroz et al., 2016; Hill et al., 2018), hippocampus
126 (Tritschler et al., 2018), or amygdala (Floresco et al., 1998). Furthermore, *in vivo* intrastriatal
127 administration of glutamate and ACh was also shown to cause increases in extracellular DA
128 concentration in the rat striatum (Giorguieff et al., 1976; Giorguieff et al., 1977; Leviel et al.,
129 1990; Shimizu et al., 1990). Altogether, this evidence supports an intrastriatal mechanism for DA
130 signal generation that can be initiated by excitatory inputs to the striatum that require glutamate
131 and ACh. While cortically evoked DA signals in the striatum have been reported, identifying the
132 unique pharmacological and basic properties of these input-specific signals will allow us to
133 selectively manipulate and target them, leading to a better understanding of their functional
134 significance. In this study, we tackle this gap in knowledge using both *in vivo* microdialysis and
135 *in vitro* FSCV with optogenetic stimulation. Particularly, we set up a novel approach using dual
136 optogenetic stimulation in the same brain slices to input-specific evoke DA release and compare
137 the properties of these DA signals in the striatum.

138 (627/650 words)

141 **Materials and Methods**

142 **Animals.** All animals used in the study were maintained in accordance with the guidelines of the
143 National Institutes of Health Animal Care and the animal research procedures were approved by
144 the NIAAA Animal Care and Use Committee for mice and by the NIDA IRP Animal Care and
145 Use Committee for rats. Except for the *in vivo* microdialysis experiments, all experiments were
146 carried out using male and female mice of C57BL/6 background. Heterozygote
147 B6.SJL-*Slc6a3^{tm1.1(cre)Bkmn}*/J mice (Backman et al., 2006)(The Jackson Laboratory, 006660)
148 referred to as DAT^{IRES-Cre+} mice and negative DAT^{IRES-Cre-} littermates considered as wild-type
149 mice were used. To fluorescently label CINs, homozygote B6N.129S6(B6)-*Chat^{tm2(cre)Lowl}*/J mice
150 (Rossi et al., 2011) (The Jackson Laboratory, 018957) were crossed with homozygote
151 B6.Cg-*Gl(ROSA)26Sor^{tm14(CAG-tdTomato)Hze}*/J mice (Madisen et al., 2010) (The Jackson Laboratory,
152 007914), and the progeny is referred to as CIN-tdTomato mice. For the microdialysis
153 experiments, male Sprague-Dawley albino rats (Charles River Laboratories, Wilmington, MA)
154 were used. Rats were housed individually for the first week after intracranial injection, until
155 suture removal, after which the rats were housed 2 per cage. All animals were housed on a 12 h
156 light/dark cycle (06:30 - 18:30 light) with food and water ad libitum.

157

158 **Surgery and stereotaxic injection of AAV-ChR2 vectors.** Injections were carried out as
159 described previously (Adrover et al., 2014). Briefly, mice (5-6 weeks old) were anesthetized by
160 inhalation of isoflurane-oxygen mixture and were placed in a stereotaxic frame (David Kopf).
161 Adeno-associated virus (AAV) vectors with Cre recombinase dependent expression of
162 Channelrhodopsin2 (ChR2) protein, AAV5-EF1a-DIO-hChR2(H134R)-EYFP (4 x 10¹² IU/ml),
163 were bilaterally injected into the ventral tegmental area/substantia nigra pars compacta

164 (VTA/SNc; AP: -3.30, ML: ± 0.60 , DV: -4.50) of DAT^{IRE5-Cre+} mice. The AAV vectors
165 AAV5-CaMKII-hChR2(H134R)-EYFP (4×10^{12} IU/ml) or AAV5-Syn-ChrimsonR-tdTomato
166 (1.7×10^{13} IU/ml), were injected in the PFC (PrL cortex, AP: +2.10, ML: ± 0.35 , DV: -2.30; IL
167 cortex, AP: +1.90, ML: ± 0.30 , DV: -3.20) of negative littermates or DAT^{IRE5-Cre+} mice. All
168 stereotaxic coordinates were from bregma (in mm) according to the mouse atlas by Franklin and
169 Paxinos (2007). 300-500 nl for VTA/SNc and 100-200 nl for PFC were injected at a flow rate of
170 100 nl/min. Recordings were made after a minimum of 4 weeks of incubation. For mice injected
171 in both VTA/SNc (DIO-ChR2-EYFP) and PFC (ChrimsonR-tdTomato), recordings were
172 performed after a minimum of 8 weeks of incubation. Viral vectors were purchased from Gene
173 Therapy Center Vector Core at University of North Carolina and Penn Vector Core at University
174 of Pennsylvania.

175

176 **Slice preparation.** Mice were anesthetized and rapidly decapitated. Brains were quickly
177 removed, mounted and sliced using a vibratome (VT-1200S Leica) in an ice-cold cutting solution
178 containing (in mM) 225 sucrose, 13.9 NaCl, 26.2 NaHCO₃, 1 NaH₂PO₄, 1.25 glucose, 2.5 KCl,
179 0.1 CaCl₂, 4.9 MgCl₂, and 3 kynurenic acid. The sagittal slices (240 μ m) were incubated for 20
180 min at 33 °C in artificial cerebrospinal fluid (ACSF) containing (in mM) 124 NaCl, 1 NaH₂PO₄,
181 2.5 KCl, 1.3 MgCl₂, 2.5 CaCl₂, 20 glucose, 26.2 NaHCO₃, and 0.4 ascorbic acid, and kept in the
182 dark at room temperature before use. Recording chamber was perfused at 2 ml/min with ACSF
183 heated at 32°C using an in-line heater (Harvard Apparatus).

184

185 **Fast-scan cyclic voltammetry (FSCV) and amperometry.** FSCV was performed in the dorsal
186 striatum. Carbon-fiber electrodes (CFEs) were prepared with a cylindrical carbon-fiber (7 μ m

187 diameter, ~150 μm of exposed fiber) inserted into a glass pipette. Before use, the CFEs were
188 conditioned with 8 ms long triangular voltage ramp (-0.4 to +1.2 and back to -0.4 V versus
189 Ag/AgCl reference at 400 V/s) delivered every 15 ms. CFEs showing current above 1.8 μA or
190 below 1.0 μA in response to the voltage ramp around 0.6 V were discarded. During the
191 recording, the CFEs were held at -0.4 V versus Ag/AgCl and the same triangular voltage ramp
192 was delivered every 100 ms. DA transients were evoked by electrical or optical single pulse, or 5
193 pulses at 20 Hz stimulations. Using the same CFE and location, DA signals were evoked by
194 alternating electrical and optical stimulations in some experiments. These data were combined
195 with results from other experiments where either electrical or optical stimulation was used to
196 evoke DA signals. For electrical stimulation, a glass pipette filled with ACSF was placed near
197 the tip of the carbon fiber and a rectangular pulse (0.2 ms, 100 μA) was applied every 2 min. For
198 optogenetic stimulation, a fiber optic (200 μm diameter, 0.22 NA, ThorLabs) connected to a blue
199 LED (470 nm, 1.8 mW of maximal output power measured at the tip of the fiber optics,
200 ThorLabs) was placed over the carbon fiber and light pulses (0.6 ms) were delivered every 2 min.
201 For input-output curves, the widths of light pulse were 0.1, 0.2, 0.5, 1, 2, and 5 ms. For dual
202 optogenetic recordings, two fiber optics connected to a purple LED (420 nm, 3.0 mW, ThorLabs)
203 and an orange LED (590 nm, 0.7 mW, ThorLabs) respectively, were placed over the carbon fiber.
204 Light pulses (0.6 ms for 420 nm and 0.6-2 ms for 590 nm) were delivered in an alternating
205 pattern every 2 min. Data were collected with a retrofit headstage (CB-7B/EC with 5 M Ω
206 resistor) using a Multiclamp 700B amplifier (Molecular Devices) after low-pass filter at 3 kHz
207 and digitized at 100 kHz using a DA board (NI USB-6229 BNC, National Instruments). Data
208 acquisition and analysis were performed using a custom-written software, VIGOR, in Igor Pro
209 (Wavemetrics) using mafPC (courtesy of M.A. Xu-Friedman). The current peak amplitudes of

210 the evoked DA transients were converted to DA concentration according to the post
211 experimental calibration using 1-3 μM DA. Amperometric recordings were performed using the
212 same carbon-fiber electrodes held at -0.4 V versus Ag/AgCl and a 30 s long step to $+0.6$ V was
213 applied. Single pulse or 5 pulses at 20 Hz stimulation were delivered at 20 s after switching to
214 $+0.6$ V. Since we did not find major differences between PrL and IL in evoking DA transients,
215 we combined the data obtained from two groups to represent DA transients evoked by PFC
216 inputs (PFC-oDA).

217

218 **Cell-attached recordings.** Striatal CINs from CIN-TdTomato mice injected with ChR2-EYFP in
219 the PFC were identified by fluorescence and confirmed by their characteristic spontaneous firing
220 pattern. Cell-attached recordings were performed from CINs in the striatum using glass pipette
221 electrodes with a resistance of $\sim 3\text{--}4$ M Ω , filled with an internal solution containing (in mM) 120
222 cesium methanesulfonate, 20 CsCl, 10 HEPES, 0.2 EGTA, 10 sodium phosphocreatine, 4 Na₂-
223 ATP, and 0.4 Na-GTP (pH, 7.25; 290–310 mOsm), at a holding potential of 0 mV. To estimate
224 the strength of connectivity to CINs, the lowest light intensity needed to reliably evoke action
225 potentials in CINs was determined, ranging from 0.4 mW for ‘high’ connectivity to 2.1 mW for
226 ‘low’ connectivity. The data were collected using a Multiclamp 700B amplifier after low-pass
227 filter at 1 kHz and digitized at 5 kHz, using pClamp10 software (Molecular Devices). Spike
228 fidelity was calculated as percentages of the number of AP evoked from 5 trials for both single
229 pulse and trains stimulation.

230

231 ***In vivo* microdialysis and optogenetic stimulation of the cortical inputs.** Rats (80-90 g)
232 received unilateral intracranial injection of AAV-CaMKIIa-hChR2(H134R)-EYFP (titer: 10^{12}

233 IU/ml; Gene Therapy Center Vector Core at University of North Carolina) in the PrL and IL
234 cortex (AP: +3.0 mm, ML: 0.5 mm, DV: -3.5 and -5 mm with respect to bregma). Two injection
235 sites per hemisphere were used and 300 nl of viral vector solution was delivered per site via a
236 105 μ m thick silica tubing injector coupled directly to a 1 μ l syringe driven by an infusion pump
237 (rate = 50 nl/min) during 10 min. The injector was left in place for an additional 10 min
238 following each injection to allow for diffusion of the suspension. Ten weeks after viral vector
239 injection, rats (350-400 g) underwent surgery for probe implantation according to previously
240 published procedures (Quiroz et al., 2016). Briefly, a modified microdialysis probe with an
241 embedded light-guiding optic fiber was implanted into the nucleus accumbens (NAc) shell (AP:
242 +1.2 mm, ML: 0.5 mm, DV: -8.0 mm with respect to bregma). The probe was fixed to the skull
243 with a stainless-steel screw and glass-ionomer dental cement. All surgical procedures were
244 performed under anesthesia with 3 ml/kg of Equithesin (4.44 g of chloralhydrate, 0.972 g of Na
245 pentobarbital, 2.124 g of MgSO₄, 44.4 ml of propylene glycol, 12 ml of ethanol and distilled
246 H₂O up to 100 ml of final solution; NIDA Pharmacy, Baltimore, MD). To build the microdialysis
247 probe with embedded optic fiber, the tip of an optic fiber (105 μ m diameter core, 0.22 Numerical
248 Aperture) was sculpted into a conical shape using a Flaming-Brown pipette puller fitted with a
249 custom platinum heating filament (Sutter Instruments, Novato, CA) to allow for a larger area of
250 stimulation. The conical optic fiber tip was embedded inside the microdialysis probe and
251 implanted. Microdialysis experiments were performed in freely moving rats 24 h after probe
252 implantation. Optical fiber was coupled to a 473 nm solid-state laser module and light
253 stimulation was driven by a Grass S88 stimulator. Light stimulation was delivered for 20 mins as
254 trains of light pulses (2 ms pulse duration; at 100 Hz for 160 ms; trains repeats once per second;
255 intensity = 5-8 mW at probe tip). ACSF containing (in mM) 144 NaCl, 4.8 KCl, 1.7 CaCl₂, and

256 1.2 MgCl₂, was pumped through the optogenetic-microdialysis probe (rate = 1.25 µl/min). After
257 a washout period of 90 min, dialysate samples were collected at 20 min intervals. After 80 min
258 of baseline sampling, optogenetic stimulation was applied for 20 min and samples were collected
259 for 80 additional minutes after the end of the stimulation. Samples were split and analyzed
260 separately for glutamate, DA and ACh content. ACh and glutamate contents were measured by
261 HPLC coupled to an ACh oxidase and glutamate oxidase enzyme reactors, respectively, and
262 electrochemical detection (Eicom Corporation). DA was measured by HPLC coupled with a
263 coulometric detector (5200a Coulochem III, ESA, Chelmsford, MA). At the end of the
264 microdialysis experiment, animals were deeply anesthetized with Equithesin and perfused
265 transcardially with 0.1 M phosphate buffered saline (PBS), followed by 4% formaldehyde in 0.1
266 M PBS, pH 7.4. Brains were postfixed in the same fixative for 2 h and immersed in 20%
267 sucrose/0.1 M PBS, pH 7.4, solution for 48 h at 4°C. Forty µm thick coronal sections were cut in
268 a Leica (Nussloch, Germany) CM3050S cryostat at -20°C, collected in PBS, and stored in
269 antifreeze-buffered solution (20% ethylene glycol, 10% glycerol, and 10% sucrose in PBS) at
270 -80°C until processing. Sections were then evaluated for localization of implanted probes and
271 ChR2-EYFP expression. Wide field images were acquired with a Typhoon laser scanner (GE
272 Healthcare). Confocal fluorescence microscopy images were acquired with a Zeiss microscope
273 (Examiner Z1, Zeiss, Gottingen, Germany) fitted with a confocal laser module (LSM-710,
274 Zeiss).

275

276 **Drugs.** Dihydro-β-erythroidine hydrobromide (DHβE) was purchased from Tocris. Kynurenic
277 acid (sodium salt), 2,3-Dioxo-6-nitro-1,2,3,4-tetrahydrobenzo[f]quinoxaline-7-sulfonamide

278 (NBQX) and 3-((*R*)-2-Carboxypiperazin-4-yl)-propyl-1-phosphonic acid (CPP) were purchased
279 from Abcam. All other chemicals were purchased from Sigma.

280

281 **Statistical analysis.** Statistical analysis was performed with Prism (GraphPad). One-sample t-
282 test, two-tailed paired t-test, repeated measures one-way (RM1W) ANOVA with or without
283 mixed-effects models (MEM), or two-way (RM2W) ANOVA were used as specified. Tukey's or
284 Dunnett's multiple comparisons test was used for post-hoc analysis as specified. The number of
285 experiments, *n*, was expressed as the number of slices or cells/the number of mice or number of
286 rats for the *in vivo* microdialysis experiments.

287 **Results**

288

289 ***In vivo* stimulation of PrL/IL inputs increases striatal ACh and DA concentration, and the**
290 **increase in DA requires nAChR activation**

291 Published work *in vivo* shows that optogenetic stimulation of cortical inputs to the
292 striatum can evoke DA release (Quiroz et al., 2016). However, this study provides no evidence
293 that activation of these cortical inputs recruits striatal CINs or that the cortically evoked DA
294 release *in vivo* require activation of striatal nAChRs. To assess these matters, we used *in vivo*
295 microdialysis combined with optogenetic stimulation, as previously described (Quiroz et al.,
296 2016), and measured extracellular levels of ACh and DA in response to optogenetic stimulation
297 of cortical inputs. A modified microdialysis probe with an embedded light-guiding optic fiber
298 was implanted into the striatum of rats expressing Chr2-EYFP in the PrL/IL cortex (Figure 1A
299 and B). On the experiment day, dialysate samples were collected at baseline for 80 min before
300 stimulation started. Optogenetic stimulation of cortical axons within the striatum was delivered
301 around the microdialysis probe as trains of light pulses (16 pulses at 100 Hz every 1 s for 20
302 mins). Samples were collected for an additional 80 mins after stimulation and were split and
303 analyzed separately for DA and ACh content or DA and glutamate. This long train of *in vivo*
304 optogenetic stimulation of PrL/IL cortical axon fibers within the striatum produced an increase in
305 extracellular concentration of DA in the striatal dialysate ($185.1 \pm 44.0\%$ of baseline, $n = 7$; $F =$
306 5.27 , $p = 0.0002$, RM1W ANOVA; $p = 0.0002$ for 60 min vs. 80 min; Dunnett's multiple
307 comparisons test; Figure 1C), which coincided with an increase of extracellular ACh
308 concentration ($196.7 \pm 36.6\%$ of baseline, $n = 7$; $F = 3.00$, $p = 0.0002$, RM1W ANOVA; $p =$
309 0.004 for 60 min vs. 80 min; Dunnett's multiple comparisons test; Figure 1D). These *in vivo*

310 microdialysis findings support the hypothesis that cortical stimulation recruits CINs. In addition,
311 when the *in vivo* optogenetic stimulation was performed in constant perfusion of the nAChR
312 antagonist DH β E (10 μ M) delivered locally via reverse dialysis, the same stimulation protocol
313 did not cause any change in extracellular DA concentration in the striatal dialysates ($96.5 \pm$
314 11.6% of baseline, $n = 9$; $F = 0.64$, $p = 0.70$, RM1W ANOVA; Figure 1E), indicating that
315 activation of nAChRs in the striatum is required for the cortically evoked DA release *in vivo*. As
316 a control, we measured glutamate concentration in these same dialysates which showed
317 increased glutamate levels and confirmed the delivery of cortical stimulation in the presence of
318 the nAChR antagonist ($184.3 \pm 27.3\%$ of baseline, $n = 9$; $F_{6,45} = 4.01$, $p = 0.003$, RM1W
319 ANOVA with MEM; $p = 0.0006$ for 60 min vs. 80 min; Dunnett's multiple comparisons test;
320 Figure 1F).

321

322 **Stimulation of PrL/IL inputs to striatum is sufficient to evoke local DA signals in brain**
323 **slices**

324 In order to precisely access the specific inputs and apply pharmacological agents, we
325 used transgenic mice with combination of optogenetic stimulation. DA signals were recorded in
326 the striatum using FSCV in mouse brain slice preparations. Release of DA from axonal
327 projections within the striatum were evoked by electrical stimulation and compared with DA
328 signals evoked by input-specific optogenetic stimulation. To achieve input-specific stimulation,
329 ChR2-EYFP was expressed in either midbrain DANs and their axonal projections to the striatum
330 using Cre-dependent viral vector injection in DAT^{ires-Cre+} mice (Figure 2A), or ChR2-EYFP in
331 cortical neurons of the PrL/IL cortex and their projections to the striatum using viral injection in
332 Cre-negative littermate mice (Figure 2B).

333 As expected, single brief pulses of electrical stimulation delivered via an electrode placed
334 within the striatal tissue reliably evoked DA (electrically evoked DA transient, eDA) signals in
335 striatal brain slices (Figure 2C). Also, direct optogenetic stimulation of midbrain DAN axonal
336 projections within the striatum also evoked DA signals (referred here as DAN-oDA) upon
337 delivery of a single brief pulse of blue light (0.6 ms), in agreement with previous published
338 studies (Adrover et al., 2014; Melchior et al., 2015). Lastly, similar to the *in vivo* findings in
339 Figure 1, selective optogenetic stimulation of axon projections from PrL/IL cortex into the
340 striatum was also sufficient to trigger DA signals (referred as PFC-oDA) in the striatum of in
341 slice preparation (Figure 2C). These PFC-oDA signals were also reliably evoked by brief single
342 pulses of blue light (0.6 ms) in the ventral portion of the dorsomedial striatum in sagittal brain
343 slices (Figure 2D). The viral expression around injection site was often large enough to include
344 both PrL and IL regions of the cortex. For this reason, we combined data from the two regions. It
345 is worth noting that these brain sections mainly contain the axon projections from PrL/IL
346 neurons but not their cell bodies, which are localized to more medial sagittal sections of the brain
347 (Figure 2B, inset).

348 The current-voltage plots of DA signals evoked via the three different types of
349 stimulation (electrical, optogenetic stimulation of DANs and optogenetic stimulation of PrL/IL)
350 were indistinguishable and displayed current peaks at the expected oxidation (0.56 ± 0.01 V for
351 eDA, $n = 15 / 8$; 0.58 ± 0.01 V for DAN-oDA, $n = 14 / 6$; 0.56 ± 0.01 V for PFC-oDA, $n = 22 /$
352 13 ; $F = 0.49$, $p = 0.62$, RM1W ANOVA with MEM; Figure 2E) and reduction voltages ($-0.17 \pm$
353 0.01 V for eDA, -0.14 ± 0.01 V for DAN-oDA, -0.16 ± 0.02 V for PFC-oDA; $F = 0.76$, $p =$
354 0.49 , RM1W ANOVA with MEM; Figure 2E) for DA. The peak amplitude of eDA was
355 significantly higher than DAN-oDA or PFC-oDA (556 ± 42 nM for eDA; 367 ± 58 nM for

356 DAN-oDA; 325 ± 23 nM for PFC-oDA; $F_{2,12} = 13.430.76$, $p > 0.05$, RM1W ANOVA with
357 MEM; $p = 0.01$ for eDA vs. DAN-oDA, $p = 0.0005$ for eDA vs. PFC-oDA, and $p = 0.99$ for
358 DAN-oDA vs. PFC-oDA; Tukey's multiple comparisons test; Figure 2F), and the decay time
359 constants (τ) were similarly longer with eDA (0.25 ± 0.01 s for eDA, 0.22 ± 0.01 s for DAN-
360 oDA, 0.23 ± 0.01 s for PFC-oDA; $F_{2,12} = 13.43$, $p = 0.0009$, RM1W ANOVA with MEM; $p =$
361 0.004 for eDA vs. DAN-oDA, $p = 0.009$ for eDA vs. PFC-oDA, and $p = 0.83$ for DAN-oDA vs.
362 PFC-oDA; Tukey's multiple comparisons test; Figure 2G). Thus, we were able to reliably evoke
363 steady DA signals by selective optogenetic stimulation of axon projections from PrL/IL cortex in
364 the ventral portion of the dorsomedial striatum. The DA signals recorded using FSCV showed
365 indistinguishable chemical and temporal characteristics, even when evoked by different inputs.

366

367 **Unique physical and pharmacological properties across input-specific DA signals**

368 We first explored the threshold for triggering the input-specific optogenetically evoked
369 DA signals. The threshold was determined by constructing input-output curves and varying the
370 light pulse durations from 0.1 to 5 ms in brain slices from mice expressing ChR2 in midbrain
371 DANs or the PrL/IL region (Figure 3A and B). The relative amplitudes of DA transients were
372 overlapping for pulses of 0.5-5 ms duration and both DAN-oDA and PFC-oDA signals showed
373 maximal amplitude with 1-5 ms light pulse durations. However, very short light pulses (0.1 ms)
374 evoked measurable DA signals only in slices in which ChR2 was expressed in midbrain DAN
375 projections to the striatum, indicating a lower threshold for evoking DA signals with direct
376 stimulation of DA neuron axons than with stimulation of cortical inputs (duration \times input, $F_{5,90} =$
377 11.58 , $p < 0.0001$, RM2W ANOVA; post hoc for the duration of 0.1 ms: $33 \pm 4\%$ for DAN-
378 oDA, $n = 12 / 8$, and $1.9 \pm 0.7\%$ for PFC-oDA, $n = 8 / 5$, $p < 0.0001$; Figure 3B). A higher

379 threshold for the cortically evoked DA signals could reflect technical differences like opsin
380 expression levels, or other biological factors such as the density of innervation of cortical vs
381 DAN axonal projections, difference in the release probability of the DA varicosities that respond
382 to direct stimulation of DAN axons from those responding to cortical inputs, and/or the indirect
383 and polysynaptic nature of the cortical-evoked DA signals.

384 To determine whether PrL/IL activation elicits striatal DA release engage the CINs
385 dependent mechanism as shown in *in vivo* microdialysis experiment (Figure 1), we then studied
386 the basic pharmacological characteristic of DA signal evoked by stimulation of PFC inputs and
387 compared them with those evoked by electrical and DAN inputs stimulation. In striatal brain
388 slices, PFC-oDA signals were completely abolished by a mixture of AMPA and NMDA
389 receptors antagonists (NBQX/ CPP), while eDA and DAN-oDA signals were unaffected
390 (amplitude after the antagonists = $0.3 \pm 1.6\%$ of baseline for PFC-oDA, $n = 6 / 5$; $107.3 \pm 3.0\%$
391 for eDA, $n = 6 / 4$; $99.8 \pm 1.4\%$ for DAN-oDA, $n = 6 / 4$; $F_{2,3} = 694.8$, $p < 0.0001$, RM1W
392 ANOVA with MEM; $p = 0.14$ for eDA vs. DAN-oDA, p 's < 0.0001 for PFC-oDA vs. eDA or
393 PFC-oDA vs. DAN-oDA; Tukey's multiple comparisons test; Figure 3C and D). These findings
394 indicate a requirement for ionotropic glutamate transmission for PrL/IL inputs to evoke local DA
395 signals, which is in agreement with previous reports on the requirement of glutamate
396 transmission for DA signals evoked by motor cortex and thalamic inputs to the striatum
397 (Threlfell et al., 2012; Kosillo et al., 2016; Cover et al., 2019). Further, similar to our *in vivo* data
398 (Figure 1D), DH β E also abolished PFC-oDA signals, and significantly depressed eDA signals,
399 while having no effect on DAN-oDA signals ($1.9 \pm 1.4\%$ of baseline for PFC-oDA, $n = 11 / 7$;
400 $21 \pm 3\%$ for eDA, $n = 10 / 5$; $99 \pm 3\%$ for DAN-oDA, $n = 5 / 2$; $F_{2,7} = 395.2$, $p < 0.0001$, RM1W
401 ANOVA with MEM; $p < 0.0001$ for eDA vs. DAN-oDA, $p = 0.0006$ for eDA vs. PFC-oDA, and

402 $p < 0.0001$ for DAN-oDA vs. PFC-oDA; Tukey's multiple comparisons test; Figure 3E and F).
403 Taken together, the pharmacology results support the hypothesis that PFC-oDA signals are
404 mediated by activation of glutamate synapses from PrL/IL cortex to striatal CINs, which excites
405 them to fire and trigger ACh release, thereby driving DA release via activation of nAChRs on
406 DAN axon fibers within the striatum.

407 ACh is rapidly cleared by enzymatic degradation by acetylcholinesterase (Quinn, 1987).
408 The extremely dense presence of acetylcholinesterase in the striatum (Zhou et al., 2001) assures
409 the termination of cholinergic action. We also have previously shown the influence of the
410 acetylcholinesterase on the DA transmission in the striatum (Shin et al., 2015; Shin et al., 2017).
411 As acetylcholinesterase activity shows temperature dependence (Vidal et al., 1987), we then
412 tested the temperature dependence of the input-specific DA transients by varying the temperature
413 of the bath solution. The amplitude of both DAN-oDA and PFC-oDA signals increased linearly
414 as the temperature was lowered from the standard 32°C to 25°C and both showed a tight
415 negative regression with similar slopes significantly different from zero ($-10.8 \pm 0.6\%$ per °C, n
416 $= 8 / 3$, for DAN-oDA, and $-10.8 \pm 2.0\%$ per °C, $n = 6 / 3$, for PFC-oDA; p 's < 0.0001 ; Figure
417 3G and H). The temperature dependence of the DA signal amplitude likely reflects the change in
418 rate of DA transporter activity with temperature. DA transporter activity was reported to have a
419 temperature coefficient Q_{10} ranging from 1.39 to 2.95 (Zhu and Hexum, 1992), from which we
420 estimate a Q_{10} of around 2.3 for the DA transporter for 24 - 37°C range. Our estimate predicts
421 that large changes in the rate of DA reuptake by the transporter would be around the tested and
422 physiological temperatures. Indeed, the decay of the DA transients, which is a parameter that
423 reflects the clearance of extracellular DA by the transporter, was also affected as the temperature
424 was lowered. The decay time constant of both DAN-oDA and PFC-oDA increased linearly with

425 the decrease of the temperature (DAN-oDA: -0.017 ± 0.001 s/°C; PFC-oDA: -0.025 ± 0.001
426 s/°C; Figure 3I), which corresponded with the linear increase in amplitude. However, raising the
427 temperature from 33°C to 35°C caused a dramatic and selective drop in the amplitude of the
428 PFC-oDA signals, compared to DAN-oDA signals (Figure 3G and H). The slope for PFC-oDA
429 signals increased 3-fold from -11% to -31% per °C.

430 Vidal et al. (1987) have reported on a high dependence with temperature of the activity of
431 acetylcholinesterase from rat brain, which reaches maximal rate around 35°C. Our *in vivo* and *in*
432 *vitro* pharmacology experiments showed that PFC-oDA signals require activation of nAChR.
433 Therefore, we speculate that the observed steep temperature dependence of the signals is in large
434 part mediated by rate increase in acetylcholinesterase activity. Furthermore, at physiological
435 temperatures the PFC-evoked DA signals may be very localized near ACh release sites,
436 presumably overlapping with nAChR expression in DAN axons.

437

438 **Activity dependent summation of the midbrain and cortical DA signals**

439 Trains of stimulation pulses has been shown to produce sublinear summation in the
440 amplitude of DA signals evoked by electrical and optogenetic stimulation of DAN axon
441 projections in the striatum *in vitro* (Zhang and Sulzer, 2004; Threlfell et al., 2010; Melchior et
442 al., 2015; Shin et al., 2017). We then tested the degree of summation of the DA signals in
443 response to short trains of stimulation pulses (5 pulses at 20 Hz) and compared it with the
444 transients evoked by a single pulse (Figure 4A and B). This pattern of train stimulation was
445 chosen based on burst firing patterns recorded *in vivo* for DANs during behavior (Schultz et al.,
446 1993; Hyland et al., 2002). Indeed, we found that trains of 5 pulses at 20 Hz evoke DA transients
447 50% larger than those evoked by single pulse stimulation for eDA signals and almost double for

448 DAN-oDA (5p/1p: 1.44 ± 0.06 , $n = 5 / 3$, for eDA; 1.92 ± 0.19 , $n = 5 / 2$, for DAN-oDA; $1.00 \pm$
449 0.02 , $n = 10 / 7$; $F_{2,2} = 110.6$, $p = 0.009$, RM1W ANOVA with MEM; $p = 0.04$ for eDA vs.
450 DAN-oDA, $p = 0.03$ for eDA vs. PFC-oDA, and $p = 0.008$ for DAN-oDA vs. PFC-oDA;
451 Tukey's multiple comparisons test; Figure 4A and B). On the contrary, PFC-oDA transients
452 evoked by this train stimulation had similar amplitudes compared to those evoked by a single
453 pulse, indicating no summation of DA signals evoked by PrL/IL inputs. In order to measure DA
454 signals with better temporal resolution, we performed amperometric recordings and again
455 compared DA signals evoked by single pulse and trains (Figure 4C). In line with the FSCV
456 results, amperometric recordings showed that DAN-oDA signals display sublinear summation
457 whereas PFC-oDA signals are indistinguishable between single pulse or trains of 5 pulses at 20
458 Hz. The lack of summation in the PFC-oDA signals in response to trains resembles the findings
459 obtained with DA signals evoked by synchronized activation of CINs (Threlfell et al., 2012; Shin
460 et al., 2017) and further supports the idea that the PFC evoked local DA signals are mediated by
461 synchronized action of CINs in response to stimulation of PrL/IL inputs. Note that the large
462 transient current deflection in response to each pulse of stimulation ($n = 5 / 4$; Figure 4C, right) is
463 suggestive of the action potential firing evoked in CINs and other striatal neurons by the
464 optogenetic stimulation of PrL/IL inputs. The fact that every pulse of the train stimulation
465 triggers a current deflection reflects the ability of PrL/IL inputs to evoke action potentials firing
466 in downstream neurons and supports the idea that the lack of summation in DA signals is not
467 likely due to the failure of action potential firing by CINs. To directly test the contribution of
468 failure of action potential firing by CINs to the lack of summation in PFC-oDA signals, we
469 carried out cell-attached recordings from CINs and measured action potential fidelity in response
470 to a single pulse and trains of 5 pulses at 20 Hz (single pulse: $96.5 \pm 2.7\%$, $n = 23 / 4$, $t = 1.28$, p

471 = 0.21; trains of 5: $81.5 \pm 7.7\%$, $n = 10 / 4$, $t = 2.42$, $p = 0.04$; both with one sample t-test to
472 100% value; Figure 4D and E). Although there was a small but significant percentage of failure,
473 the totality of the data indicate that the lack of summation is not likely caused by action potential
474 failure, but instead can be attributed to other downstream mechanisms such as desensitization of
475 nAChRs (Threlfell et al., 2012; Shin et al., 2017).

476

477 **Input-specific DA signals are evoked by dual optogenetic stimulation in the same brain**
478 **slice**

479 Thus far, DA signals evoked by the different inputs were recorded in brain slices from
480 different mice that expressed ChR2 in either midbrain DANs or in PrL/IL cortex. In order to
481 strictly test the segregation/distinction of these two pathways, it was important to examine these
482 two inputs and compare the input-specific DA signals in the slice preparation from the same
483 mice. We took advantage of opsins activated by different light wavelengths, specifically, ChR2
484 and the red-shifted opsin ChrimsonR (Klapoetke et al., 2014). We first set up the conditions for
485 selective stimulation of each opsin without cross-activation. In brain slices expressing only ChR2
486 in midbrain DANs, pulses of purple light (420 nm) evoked reliable DA signal while similar and
487 longer pulses of orange light (590 nm) did not trigger any detectable signals (Figure 5A).
488 Conversely, in slices expressing only ChrimsonR in the PrL/IL cortex, brief orange light pulses
489 evoked DA signal, but not purple light (Figure 5B). Thus, under these experimental conditions,
490 ChR2 and ChrimsonR can be used in combination to selectively stimulate two different inputs by
491 delivering pulses of two different light wavelengths without any detectable cross- activation.

492 Next, in the same $DAT^{IRES-Cre+}$ mice, ChR2-YFP was expressed in midbrain DANs with a
493 Cre-dependent expression vector and ChrimsonR-TdTomato was expressed in PrL/IL cortex.

494 Figure 5C shows examples of the fluorescent expression pattern of ChR2-YFP (green) and
495 ChrimsonR (red) in the same sagittal brain slice from this double-injected mouse. Figure 5D
496 shows the experimental arrangement for the dual input recordings with the placement of the
497 carbon fiber and the two fiber-optics for delivering the purple and orange light pulses that were
498 used to activate ChR2 and ChrimsonR, respectively. In these slices with dual opsin expression,
499 brief pulses of either purple or orange light evoked DA signals with indistinguishable current-
500 voltage plots showing the characteristic peaks for DA oxidation and reduction (Figure 5E). The
501 DA concentration transients had comparable peak amplitudes with means of 407 ± 32 nM for
502 DAN-oDA and 420 ± 36 nM for PFC-oDA ($n = 43 / 13$, $t = 0.47$, $df = 42$, $p = 0.64$, paired t-test;
503 Figure 5F) and overlapping time courses as measured at 10 Hz sample rate of FSCV, in
504 agreement with the results shown in Figure 2. The decay time constant of the DA transients were
505 similar (0.28 ± 0.01 s for DAN-oDA and 0.28 ± 0.01 s for PFC-oDA, $n = 43 / 13$, $t = 0.41$, $df =$
506 41 , $p = 0.68$ from paired t-test; Figure 5F).

507 Then, we tested the pharmacological properties of DAN-oDA and PFC-oDA by
508 delivering alternating purple and orange light pulses and recording from a single carbon fiber.
509 Application of the glutamate receptor antagonists NBQX/CPA ($99.2 \pm 3.1\%$ of the baseline for
510 DAN-oDA and $1.6 \pm 1.1\%$ for PFC-oDA, $n = 5 / 3$; $t = 25.3$, $df = 4$, $p < 0.0001$, two-tailed paired
511 t-test; Figure 5G) or the nAChR antagonist DH β E ($101.9 \pm 0.6\%$ of the baseline for DAN-oDA
512 and $0.8 \pm 0.8\%$ for PFC-oDA, $n = 5 / 3$; $t = 79.13$, $df = 4$, $p < 0.0001$, two-tailed paired t-test;
513 Figure 5H) completely abolished PFC-oDA signals while leaving DAN-oDA signals in the same
514 location intact. These results confirm the findings from Figure 3, which use antagonists and
515 single input optogenetic stimulation to evoke either DAN-oDA or PFC-oDA in separate
516 slices/mice. These results also validate the experimental approach by showing input specificity

517 with no apparent crossover in the optogenetic stimulation of ChR2 and ChrimsonR with the
518 described wavelengths. More importantly, these pharmacological findings highlight the different
519 mechanisms and the unique nature of the input-specific DA signals evoked by PFC and midbrain
520 inputs.

521

522 **Cortically evoked signals are spatially restricted**

523 As shown in Figure 2D, DA signals evoked by selective stimulation of PrL/IL inputs
524 were preferentially detected between the nucleus accumbens core and dorsal striatum. We then
525 set out to investigate in more detail the spatial distribution of the input-specific DA signals using
526 the dual-opsin expression approach by sampling the amplitude of DA signals across 18 different
527 striatal areas of the sagittal brain slice while evoking responses with purple and orange light.
528 While DAN-oDA signals were detected throughout the whole striatum, PFC-oDA signals were
529 spatially restricted (Figure 6A and B). Both DAN-oDA and PFC-oDA signals showed significant
530 correlations with the fluorescent intensity of the projections ($p = 0.03$ and $r^2 = 0.28$ for DAN-
531 oDA; $p = 0.01$, $r^2 = 0.37$ for PFC-oDA; Figure 6B). However, the slope of the linear regression
532 was larger for DAN-oDA signals than PFC-oDA signals (10 vs 6 nM/AU, respectively; Figure
533 6B). Thus, the intensity of the DAN labeled fibers was a good predictor of the magnitude of
534 DAN-oDA signals. On the other hand, the presence of cortical axon fluorescence was not always
535 a predictor of PFC-oDA signals, likely due to the larger density of passing cortical axons that are
536 not synaptic terminal run through the striatum.

537 Averaging the area responses in 5 brain slices from 3 mice, we found that the mean
538 amplitude of the PFC-oDA signals was largest in the ventral part of the dorsal striatum, which
539 again maps in gross terms with the location of the brightest intensity of ChR2-EYFP labeled

540 projections from PrL/IL cortex (Figure 6C and D). However, the correlation between
541 fluorescence intensity and amplitude of PFC-oDA signals is not always strong and, for example,
542 the more intensely labeled caudal areas near the globus pallidus show almost no PFC-oDA signal
543 (Figure 6C and D). The evidence of small or no PFC-oDA signals in the more caudal striatum
544 could possibly reflect greater fiber density rather than innervation of the caudal portion of the
545 striatum by the axonal projections from PrL/IL cortex.

546 The number of CINs is less than 1% of the total striatal neurons and they are sparsely
547 distributed throughout the striatum (Burke et al., 2017). We then quantified the density of CINs
548 from the same area to further determine whether the distribution of CINs contribute to the spatial
549 restriction of PFC-oDA signals. For this purpose, we took advantage of CIN-tdTomato mouse
550 line which fluorescently labels CINs throughout the striatal slices (Figure 6E). The quantification
551 analysis of cell numbers in $400 \times 400 \mu\text{m}^2$ showed that the density of CINs was also highest in
552 the middle part of the dorsomedial striatum (6 slices from 3 mice), suggesting that an uneven
553 distribution of CINs could also contribute to the spatial restriction of the local DA signals evoked
554 by PrL/IL cortical inputs to the ventral portion of the dorsomedial striatum. To further test
555 whether the spatial profile of PFC-oDA signals is in part determined by the strength of the
556 innervation of CINs by PrL/IL cortical neurons, we performed cell-attached recordings from the
557 same CINs of CIN-TdTomato mice and measured the ability of PFC optogenetic stimulation to
558 evoke action potentials in CINs throughout the striatum (46 CINs from 3 mice). We found that
559 the connectivity followed a similar pattern to the PFC-oDA profile, and the probability that CINs
560 will fire an action potential in response to PFC stimulation was higher in the central part of the
561 striatum than in the nucleus accumbens and dorsal regions of the dorsal striatum (Figure 6F).

562 In conclusion, this study offers a series of *in vitro* and *in vivo* evidence that stimulation of
563 cortical inputs from the PrL/IL cortex can evoke DA release in the striatum via a local
564 mechanism that recruits CINs and requires activation of nAChRs. Since these cortically evoked
565 DA signals are spatially restricted and have different properties, we speculate that they are
566 engaged in distinctive striatal functions from those assigned for DA signals evoked by midbrain
567 DANs.
568
569

570 **Discussion**

571 This study provides strong evidence that DA signals in the striatum can occur both *in*
572 *vivo* and *in vitro* in response to stimulation of PrL/IL cortical inputs. These PrL/IL evoked DA
573 signals have distinctive pharmacological and physiological properties, compared to the DA
574 signals evoked by DAN inputs. The *in vitro* experiments also introduce a dual optogenetic
575 stimulation approach with which we can activate two different inputs to the striatum in the same
576 brain slice, without apparent cross-activation. This study further reveals the spatial localization
577 of the DA signals evoked by PFC inputs.

578 We showed that the PrL/IL evoked DA signals require activation of glutamate and
579 nicotinic ACh receptors, in line of a series of elegant published work. Using *in vitro* radioactive
580 assays and *in vivo* microdialysis, it was first shown that locally administered ACh and glutamate
581 can trigger DA release in the striatum (Giorguieff et al., 1976; Giorguieff et al., 1977).
582 Giorguieff and coauthors (1976) showed that an nAChR antagonist blocked ACh-evoked DA
583 signals, and speculated that "...the release of DA from dopaminergic terminals can be regulated
584 by cholinergic presynaptic receptors exhibiting nicotinic characteristics." To their credit, their
585 conclusions agree with our interpretations of the findings from the current study as well as other
586 recent optogenetic studies where it was shown that selective stimulation of CINs is sufficient to
587 evoke DA signals (Cachope et al., 2012; Threlfell et al., 2012; Wang et al., 2014; Shin et al.,
588 2017). The involvement of CINs in the glutamate-dependent DA signals was also suggested by
589 early work by Taber and Fibiger (1994) who showed that electrical stimulation of PFC can
590 increase levels of ACh in the striatum and further supported by more recent optogenetic studies
591 (Threlfell et al., 2012; Kosillo et al., 2016; Johnson et al., 2017; Mateo et al., 2017; Cover et al.,
592 2019).

593 Here, our experiments confirmed the requirement for ionotropic glutamate receptor
594 activation in the PFC-evoked DA signals as previously shown (Mateo et al., 2017). We also
595 show that nAChRs are required for the PrL/IL evoked DA signals *in vitro*, similar to other
596 findings when stimulating inputs from other cortical (Kosillo et al., 2016) and thalamic areas
597 (Threlfell et al., 2012; Kosillo et al., 2016; Cover et al., 2019) and indirectly *in vivo* (Mateo et al.,
598 2017). Our results from the *in vivo* microdialysis experiments reproduce the original findings
599 from Quiroz et al. (2016) showing that optogenetic stimulation of PFC inputs increases striatal
600 levels of DA *in vivo* (and glutamate, as expected, Figure 1). More importantly, we showed that
601 stimulation of PrL/IL inputs to the striatum also elevates striatal levels of ACh *in vivo* and that
602 this cortically evoked DA signals are blocked when a nAChR antagonist is perfused (Figure 1C
603 and D). Thus, these findings support that idea PrL/IL inputs form excitatory synapses on striatal
604 CINs and can activate them to evoke ACh release (Figure 1C). In agreement with this conclusion,
605 recent work showed that optogenetic stimulation of either M1 motor cortex or parafascicular
606 nucleus of the thalamus can induce release of ACh that was detected using exogenous G-protein
607 coupled inward rectifying K-current expressed in medium spiny neurons (Mamaligas et al.,
608 2019). Taken together, our findings from both *in vitro* and *in vivo* strongly support the
609 hypothesis of a local mechanism for evoking DA release in the striatum, in addition to the more
610 conventional mechanism based on midbrain DAN firing. This local mechanism engages striatal
611 CINs, the targets of inputs from PFC, which have an essential role in evoking DA release from
612 DAN fibers.

613 DA signals evoked by PrL/IL inputs and those evoked by DAN fibers stimulation share
614 common properties such as overlapping electrochemical profiles of the voltammetric currents
615 and similar concentration range, time course and decay time constant of the signals (Figure 2,

616 Figure 5E and F). However, there are also several differences between the input-specific DA
617 signals. First, DANs evoked DA signals do not require activation of either ionotropic glutamate
618 receptors or nAChRs (Figure 3C-F, Figure 5G and H), confirming the direct nature of this
619 mechanism that is triggered by ChR2 evoked action potentials in DAN axon fibers. Second,
620 PrL/IL evoked DA signals display different temperature sensitivity and a higher threshold
621 compared to DAN-oDA requiring a longer duration of light stimulation as determined in the
622 input-output relationship (Figure 3 and 4). This finding may reflect the poly-synaptic nature of
623 the cortically evoked signals and the requirement of synchronized activation of CINs in order to
624 trigger DA release by this local mechanism (Threlfell et al., 2012; Kosillo et al., 2016; Liu et al.,
625 2018). Third, the amplitude of DANs evoked DA signals increases as the number of stimulation
626 pulses increases, indicating some summation in the DA signals evoked by a train of stimulation
627 pulses (Figure 4A and B). In contrast, the amplitude of DA signals in response to a train of
628 pulses of cortical input stimulation is similar to the amplitudes obtained in response to a single
629 pulse of stimulation, indicating no summation under this condition for the local mechanism
630 (Figure 4A and B). ChR2 displays use-dependent inactivation when stimulated at high frequency
631 (Hass and Glickfeld, 2016). However, the lack of summation by the train stimulation is unlikely
632 due to this use-dependent inactivation of ChR2 since 20 Hz train stimulation was still able to
633 evoke action potentials in CINs recorded in cell attached mode (Figure 4D and E) and
634 amperometry recording showed large deflections in response to train stimulation (Figure 4C).
635 Anecdotally, these current deflections disappeared when the ionotropic glutamate receptor
636 antagonists were applied, also supporting the idea that firing in CINs and other downstream
637 neurons occurs in response to 20 Hz train stimulation. The lack of summation was also reported
638 in DA signals evoked by direct optogenetic stimulation of CINs in the dorsal striatum (Threlfell

639 et al., 2012; Shin et al., 2017), which was suggested to be due to nAChRs desensitization. We
640 speculate then that the lack of summation we report here by 20 Hz trains in PrL/IL evoked DA
641 signals, which also require nAChRs activation, is also due to desensitization.

642 To directly study and compare the input-specific DA signals in the same animal, we
643 established dual optogenetic stimulation using a red-shifted opsin, ChrimsonR, in combination
644 with the blue-light activated ChR2. Two wavelengths for excitation were chosen based on the
645 excitation spectrum of each opsin (Klapoetke et al., 2014), 590 nm for ChrimsonR and 420 nm
646 for ChR2, which showed no cross-activation (Figure 5A and B). This dual optogenetic approach
647 was further validated using pharmacology in animals expressing ChR2 in midbrain DANs and
648 ChrimsonR in PrL/IL neurons. We found that PrL/IL evoked DA signals were completely
649 blocked by antagonists of either ionotropic glutamate receptors or nAChRs, without affecting
650 DAN-oDA signals in the same slice (Figure 5G and H). Therefore, we determined that the two
651 inputs can be activated independently using this dual optogenetic approach in brain slices from
652 the same animal.

653 Interestingly, using this dual optogenetic approach, an intriguing spatial pattern was
654 revealed for the cortically evoked PrL/IL DA signals. While DAN-oDA signals were recorded
655 throughout the striatum, PrL/IL oDA signals were spatially restricted to a “hot-spot” region
656 around the boundary between the nucleus accumbens core and dorsal medial striatum (Figure 6).
657 This hot-spot area for the PrL/IL oDA signals corresponds to the same area where we found the
658 highest density of CINs in our analysis. Thus, CIN density could contribute in part to the
659 generation of this hot-spot area for the PrL/IL evoked DA signals. Further, we also found that
660 this area has the highest intensity of fluorescently labeled PrL/IL fibers, as well as the highest
661 degree of synaptic connections to CINs, which is also in agreement with reported patterns of

662 cortical connectivity (Voorn et al., 2004). Our initial interest was to study the PFC projections to
663 the accumbens. However, since PrL/IL evoked DA signals were largest and more reliable in the
664 ventral DS (Figure 6), recordings were performed in this area. Altogether, these findings suggest
665 that PrL/IL inputs and the synaptic innervation to CINs are preferentially localized to the
666 dorsomedial subregion, giving rise to the largest cortically evoked DA signals.

667 From the mechanism described here for this PrL/IL evoked DA signals, we propose that
668 any input to the striatum that strongly activates CINs (cortical, thalamic, or any other brain
669 region) can in theory evoke local DA signals in the striatum. We also speculate, based on ours
670 and other groups' works, that these glutamate-driven DA signals can similarly happen in other
671 striatal subregions. The selective localization of PrL/IL evoked DA signals suggests the
672 existence of a “topographic map” for the local DA signals where inputs from different cortical
673 subregions can trigger local DA signals at the striatal subregion which they innervate. Spatial
674 segregation of input-specific DA signals in the striatum is a new concept introduced here that is
675 rarely considered in the field. This concept may become helpful in understanding how DA
676 signals in the striatum can be involved in so many diverse processes ranging from reinforcement
677 learning and motivation to motor output and action selection.

678 (1499/1500 words)

679

680 **Figure legends**

681

682 **Figure 1. Effect of the nAChR antagonist DH β E on the extracellular DA level evoked by**
683 **local optogenetic stimulation of PFC fibers *in vivo*.**

684 **A.** A diagram showing the injection of Chr2-EYFP in the PrL and IL cortices (green circle) and
685 projection to the striatum with the microdialysis-optogenetics probe in a sagittal brain view. **B.**
686 Left, optogenetic-microdialysis probe schematics; a. liquid inlet, b. dialysis membrane, c. liquid
687 outlet, d. sculpted optic fiber. Middle, probe tip detail. Scale bar: 0.2 mm. Right, a picture of the
688 optogenetic-microdialysis probe showing light spread pattern at the probe tip. Scale bar: 1 mm.

689 **C-D.** Time course of extracellular concentrations of **(C)** DA (red) and **(D)** ACh (black) in the
690 NAc. **E-F.** Time course of extracellular concentrations of **(E)** DA (red) and **(F)** glutamate (Glu,
691 green) in the NAc with constant perfusion (reverse dialysis) of the nAChR antagonist DH β E (10
692 μ M). Time 0-60 represents the values of samples before stimulation; the period of optogenetic
693 stimulation (20 min) is represented as a train of blue vertical lines. Results are expressed as mean
694 \pm SEM of percentage of the average of three values before stimulation. * $p < 0.05$, ** $p < 0.01$,
695 *** $p < 0.001$.

696

697 **Figure 2. Striatal DA signals evoked by midbrain and cortical inputs.**

698 **A.** Example of the fluorescence pattern (bottom) observed in a sagittal brain slice from a
699 DAT^{IRES-Cre+} mice injected with DIO-ChR2-EYFP in the midbrain (top). **B.** Example of the
700 fluorescence pattern (bottom) observed in a sagittal brain slice from a C57Bl6/J (DAT^{IRES-Cre-})
701 mice injected with Chr2-EYFP in the PrL or IL cortex (top). The inset shows a more medial
702 slice with the site of injection. **C.** Representative DA transients, current-voltage (CV) plots and

703 color voltammograms when evoked by electrical stimulation (eDA, left), optogenetic stimulation
704 of DAN fibers (DAN-oDA, middle), or optogenetic stimulation of PFC inputs (PFC-oDA, right).
705 All three CV plots show the electrochemical profile of DA oxidation. Scalebars: 100 nM. **D.** A
706 sagittal brain section modified from The Mouse Brain Atlas (Franklin and Paxinos, 2007)
707 showing the FSCV recording sites from mice injected with Chr2-EYFP in the PrL (filled) and
708 IL (empty) cortex. **E.** The oxidation (top) and reduction (bottom) voltages from the CV plots of
709 eDA (left), DAN-oDA (middle), and PFC-oDA (right) were plotted as averages with SEMs. The
710 open and filled circles represent individual values. **F-G.** **(F)** DA peak concentrations and **(G)**
711 decay time constants of eDA (left), DAN-oDA (middle), and PFC-oDA (right) were plotted as
712 averages with SEMs. The open circles represent individual values. For PFC-oDAs, the same
713 color code was applied as in (D) for PrL and IL according to injection location. Data points in E-
714 G include experiments where electrical and optogenetic stimulation were delivered alternately
715 in the same slice or in different slices (see Materials and Methods). ** $p < 0.01$, *** $p < 0.001$.
716 LV: lateral ventricle, DS: dorsal striatum, ac: anterior commissure, AcC: accumbens core, AcSh:
717 accumbens shell, VP: ventral pallidum, PBP: parabrachial pigmented nucleus, SNR: substantia
718 nigra reticulata, Th: thalamus, Tu: olfactory tubercle.

719

720 **Figure 3. DAN-oDA and PFC-oDA show different physical and pharmacological**
721 **properties.**

722 **A.** Representative DAN-oDA (left) and PFC-oDA (right) transients evoked with different light
723 pulse duration (in ms). Scalebars: 100 nM, 0.5 s. **B.** oDA amplitudes normalized to their
724 maximum response were averaged and plotted as a function of the stimulus duration. **C.**
725 Representative traces of eDA, DAN-oDA, and PFC-oDA transients before and after bath

726 application of the glutamate receptor antagonists, NBQX and CPP (both 5 μ M). The dotted line
727 (upper) represents the amplitude of DA transients before the drugs. Scalebars: 200 nM, 2 s. **D.**
728 Averages with SEM of DA amplitude after NBQX and CPP were plotted. The open circles
729 represent individual value. **E.** Representative traces of eDA, DAN-oDA, and PFC-oDA
730 transients before and after bath application of the β 2-contatining nAChR antagonist, DH β E (1
731 μ M). Scalebars: 200 nM, 2 s. **F.** Averages with SEM of DA amplitude after DH β E were plotted.
732 The open circles represent individual value. *** vs. DAN-oDA, ### vs. eDA. **G.** Representative
733 traces of DAN-oDA (left) and PFC-oDA (right) transients at 25, 32, and 35°C. The dotted line
734 (upper) represents the oDA amplitude at 32°C. Scalebars: 200 nM, 2 s. **H.** Average oDA peak
735 amplitudes normalized to 32°C and **I.** average oDA decay time constants were plotted as a
736 function of temperature. * $p < 0.05$, *** and ### $p < 0.001$.

737

738 **Figure 4. PFC-oDA shows no summation by train stimulations.**

739 **A.** Representative DA traces of eDA, DAN-oDA, and PFC-oDA transients evoked by single
740 pulse (1p, thin traces) or train of 5 pulses at 20 Hz (5p, thick traces). Scale bars: 200 nM, 2 s. **B.**
741 Averages with SEM of the DA amplitude ratio (5p/1p) for eDA, DAN-oDA, and PFC-oDA
742 transients were plotted. The open circles represent individual values. **C.** Representative
743 amperometric traces for DAN-oDA (left) and PFC-oDA (right) transients evoked by single pulse
744 (grey traces) or train of 5 pulses at 20 Hz (color traces). PFC-oDA amperometric transients
745 evoked by 5p at 20 Hz were indistinguishable from 1p stimulation, except the large deflection at
746 the stimulation time for 5p pulses. Scale bars: 200 pA, 100 ms. **D.** Representative cell-attached
747 recordings from CINs with single (top, grey) or train of 5 pulses at 20 Hz (bottom, green). Scale

748 bars: 20 pA, 100 ms. **E.** Averages with SEM of the action potential fidelity were plotted for the
749 single pulse and train stimulation. The open circles represent individual values. **** $p < 0.0001$.

750

751 **Figure 5. Dual opsin expression to evoke cortical and midbrain DA signals in the same**
752 **brain slices.**

753 **A, B.** Left, Representative traces of DA signals evoked by either 420 nm or 590 nm light pulses
754 from mice expressing **(A)** only ChR2 in midbrain DANs or **(B)** only ChrimsonR in PrL/IL
755 cortex. Right, oDA amplitudes were plotted as pairs for each wavelength. **C.** Example of the
756 fluorescence patterns with filter set for yellow signal (left) or red signal (right) from a sagittal
757 brain slice of a DAT^{IRRES-Cre+} mice injected with ChrimsonR-TdTomato in the PFC and DIO-
758 ChR2-EYFP in the midbrain. **D.** Configuration to the FSCV DA recording using a carbon fiber
759 and two fiber optics delivering 420 nm and 590 nm, respectively. **E.** Representative DA
760 transients, CV plots and color voltammograms of DAN-oDA and PFC-oDA. **F.** Left, Amplitudes
761 were plotted as pairs for DAN-oDA and PFC-oDA recorded from same slices. Right, Averages
762 with SEM of decay time constant were plotted for DAN-oDA and PFC-oDA. The dots represent
763 individual values. **G.** Left, Representative traces of DAN-oDA (top) and PFC-oDA (bottom)
764 before and after the application of glutamate receptor antagonists NBQX and CPP. Right,
765 Averages with SEM of DAN-oDA and PFC-oDA were plotted as a function of time as
766 NBQX/ CPP was applied. **H.** Left, Representative traces of DAN-oDA (top) and PFC-oDA
767 (bottom) before and after the application of nAChR antagonists DH β E. Right, Averages with
768 SEM of DAN-oDA and PFC-oDA were plotted as a function of time as DH β E was applied.

769

770 **Figure 6. Cortically evoked DA signals are spatially restricted.**

771 **A.** The locations of carbon fiber and two fiber optics were adjusted to measure DAN-oDA (left)
772 and PFC-oDA (right) from each location where the corresponding oDA's were superimposed on
773 the fluorescence patterns. Scale bars: 500 μm . **B.** Peak amplitudes of DAN-oDA (top) and PFC-
774 oDA (bottom) were plotted as a function of fluorescence intensity at each location shown in **(A)**.
775 The dotted lines represent linear regression between the oDA amplitudes and the fluorescence
776 intensities. **C.** PFC-oDAs were measured from 74 locations (around between 1.0 and 1.2 mm in
777 ML coordinate) of mice injected with Chr2-EYFP in PrL/IL cortex and color-coded according
778 to their peak DA concentrations. The average PFC-oDA amplitudes were calculated and color-
779 coded for the three sub-regions. **D.** The PFC inputs fluorescence intensities were color-coded for
780 the same 74 locations in **(C)**. The averages from the three sub-regions were calculated and color-
781 coded. **E.** Left, Fluorescence image of striatal CINs labeled with td-Tomato. (Inset) Examples of
782 identified CINs (red) from the area with the dotted yellow line. Right, the average numbers of
783 CINs per $400 \times 400 \mu\text{m}^2$ (area as shown in the inset) were calculated and shown for the three sub
784 regions. **F.** Using cell-attached patch recording, action potentials evoked by PFC stimulation
785 were observed from a total of 46 CINs. For each CIN, a minimum light intensity to evoke action
786 potentials was determined to score the connectivity. The white circles with a thicker line
787 represent CINs which did not show any evoked action potentials even with the maximum light
788 intensity.

789

790

791

792

793

References

- 795
796
797 Adrover MF, Shin JH, Alvarez VA (2014) Glutamate and dopamine transmission from midbrain
798 dopamine neurons share similar release properties but are differentially affected by
799 cocaine. *The Journal of neuroscience : the official journal of the Society for Neuroscience*
800 34:3183-3192.
- 801 Backman CM, Malik N, Zhang Y, Shan L, Grinberg A, Hoffer BJ, Westphal H, Tomac AC
802 (2006) Characterization of a mouse strain expressing Cre recombinase from the 3'
803 untranslated region of the dopamine transporter locus. *Genesis* 44:383-390.
- 804 Burke DA, Rotstein HG, Alvarez VA (2017) Striatal Local Circuitry: A New Framework for
805 Lateral Inhibition. *Neuron* 96:267-284.
- 806 Cachope R, Mateo Y, Mathur BN, Irving J, Wang HL, Morales M, Lovinger DM, Cheer JF
807 (2012) Selective activation of cholinergic interneurons enhances accumbal phasic
808 dopamine release: setting the tone for reward processing. *Cell reports* 2:33-41.
- 809 Chuhma N, Mingote S, Moore H, Rayport S (2014) Dopamine neurons control striatal
810 cholinergic neurons via regionally heterogeneous dopamine and glutamate signaling.
811 *Neuron* 81:901-912.
- 812 Cover KK, Gyawali U, Kerkhoff WG, Patton MH, Mu C, White MG, Marquardt AE, Roberts
813 BM, Cheer JF, Mathur BN (2019) Activation of the Rostral Intralaminar Thalamus
814 Drives Reinforcement through Striatal Dopamine Release. *Cell reports* 26:1389-1398
815 e1383.
- 816 Floresco SB, Yang CR, Phillips AG, Blaha CD (1998) Basolateral amygdala stimulation evokes
817 glutamate receptor-dependent dopamine efflux in the nucleus accumbens of the
818 anaesthetized rat. *The European journal of neuroscience* 10:1241-1251.
- 819 Franklin KBJ, Paxinos G (2007) *The mouse brain in stereotaxic coordinates*, 3rd ed Edition.
820 Amsterdam: Elsevier.
- 821 Gerfen CR (2000) Dopamine-mediated gene regulation in models of Parkinson's disease. *Ann*
822 *Neurol* 47:S42-50; discussion S50-42.
- 823 Gerfen CR, Surmeier DJ (2011) Modulation of striatal projection systems by dopamine. *Annu*
824 *Rev Neurosci* 34:441-466.
- 825 Giorgiueff MF, Kemel ML, Glowinski J (1977) Presynaptic effect of L-glutamic acid on the
826 release of dopamine in rat striatal slices. *Neuroscience letters* 6:73-77.
- 827 Giorgiueff MF, Le Floc'h ML, Westfall TC, Glowinski J, Besson MJ (1976) Nicotinic effect of
828 acetylcholine on the release of newly synthesized (3H)dopamine in rat striatal slices and
829 cat caudate nucleus. *Brain research* 106:117-131.

- 830 Hass CA, Glickfeld LL (2016) High-fidelity optical excitation of cortico-cortical projections at
831 physiological frequencies. *Journal of neurophysiology* 116:2056-2066.
- 832 Hill DF, Parent KL, Atcherley CW, Cowen SL, Heien ML (2018) Differential release of
833 dopamine in the nucleus accumbens evoked by low-versus high-frequency medial
834 prefrontal cortex stimulation. *Brain Stimul* 11:426-434.
- 835 Hyland BI, Reynolds JN, Hay J, Perk CG, Miller R (2002) Firing modes of midbrain dopamine
836 cells in the freely moving rat. *Neuroscience* 114:475-492.
- 837 Johnson KA, Mateo Y, Lovinger DM (2017) Metabotropic glutamate receptor 2 inhibits
838 thalamically-driven glutamate and dopamine release in the dorsal striatum.
839 *Neuropharmacology* 117:114-123.
- 840 Klapoetke NC et al. (2014) Independent optical excitation of distinct neural populations. *Nat*
841 *Methods* 11:338-346.
- 842 Kosillo P, Zhang YF, Threlfell S, Cragg SJ (2016) Cortical Control of Striatal Dopamine
843 Transmission via Striatal Cholinergic Interneurons. *Cerebral cortex*.
- 844 Lahiri AK, Bevan MD (2020) Dopaminergic Transmission Rapidly and Persistently Enhances
845 Excitability of D1 Receptor-Expressing Striatal Projection Neurons. *Neuron* 106:277-290
846 e276.
- 847 Leviel V, Gobert A, Guibert B (1990) The glutamate-mediated release of dopamine in the rat
848 striatum: further characterization of the dual excitatory-inhibitory function. *Neuroscience*
849 39:305-312.
- 850 Liu C, Kaeser PS (2019) Mechanisms and regulation of dopamine release. *Current opinion in*
851 *neurobiology* 57:46-53.
- 852 Liu C, Kershberg L, Wang J, Schneeberger S, Kaeser PS (2018) Dopamine Secretion Is
853 Mediated by Sparse Active Zone-like Release Sites. *Cell* 172:706-718 e715.
- 854 Luscher C, Robbins TW, Everitt BJ (2020) The transition to compulsion in addiction. *Nature*
855 *reviews Neuroscience* 21:247-263.
- 856 Madisen L, Zwingman TA, Sunkin SM, Oh SW, Zariwala HA, Gu H, Ng LL, Palmiter RD,
857 Hawrylycz MJ, Jones AR, Lein ES, Zeng H (2010) A robust and high-throughput Cre
858 reporting and characterization system for the whole mouse brain. *Nature neuroscience*
859 13:133-140.
- 860 Mamaligas AA, Cai Y, Ford CP (2016) Nicotinic and opioid receptor regulation of striatal
861 dopamine D2-receptor mediated transmission. *Sci Rep* 6:37834.
- 862 Mamaligas AA, Barcomb K, Ford CP (2019) Cholinergic Transmission at Muscarinic Synapses
863 in the Striatum Is Driven Equally by Cortical and Thalamic Inputs. *Cell reports* 28:1003-
864 1014 e1003.

- 865 Mateo Y, Johnson KA, Covey DP, Atwood BK, Wang HL, Zhang S, Gildish I, Cachope R,
866 Bellocchio L, Guzman M, Morales M, Cheer JF, Lovinger DM (2017) Endocannabinoid
867 Actions on Cortical Terminals Orchestrate Local Modulation of Dopamine Release in the
868 Nucleus Accumbens. *Neuron* 96:1112-1126 e1115.
- 869 Matsuda W, Furuta T, Nakamura KC, Hioki H, Fujiyama F, Arai R, Kaneko T (2009) Single
870 nigrostriatal dopaminergic neurons form widely spread and highly dense axonal
871 arborizations in the neostriatum. *The Journal of neuroscience : the official journal of the*
872 *Society for Neuroscience* 29:444-453.
- 873 Melchior JR, Ferris MJ, Stuber GD, Riddle DR, Jones SR (2015) Optogenetic versus electrical
874 stimulation of dopamine terminals in the nucleus accumbens reveals local modulation of
875 presynaptic release. *J Neurochem* 134:833-844.
- 876 Quinn DM (1987) Acetylcholinesterase - Enzyme Structure, Reaction Dynamics, and Virtual
877 Transition-States. *Chem Rev* 87:955-979.
- 878 Quiroz C, Orru M, Rea W, Ciudad-Roberts A, Yepes G, Britt JP, Ferre S (2016) Local Control
879 of Extracellular Dopamine Levels in the Medial Nucleus Accumbens by a Glutamatergic
880 Projection from the Infralimbic Cortex. *The Journal of neuroscience : the official journal*
881 *of the Society for Neuroscience* 36:851-859.
- 882 Rossi J, Balthasar N, Olson D, Scott M, Berglund E, Lee CE, Choi MJ, Lauzon D, Lowell BB,
883 Elmquist JK (2011) Melanocortin-4 receptors expressed by cholinergic neurons regulate
884 energy balance and glucose homeostasis. *Cell Metab* 13:195-204.
- 885 Schultz W, Apicella P, Ljungberg T (1993) Responses of monkey dopamine neurons to reward
886 and conditioned stimuli during successive steps of learning a delayed response task. *The*
887 *Journal of neuroscience : the official journal of the Society for Neuroscience* 13:900-913.
- 888 Shimizu N, Duan SM, Hori T, Oomura Y (1990) Glutamate modulates dopamine release in the
889 striatum as measured by brain microdialysis. *Brain Res Bull* 25:99-102.
- 890 Shin JH, Adrover MF, Alvarez VA (2017) Distinctive Modulation of Dopamine Release in the
891 Nucleus Accumbens Shell Mediated by Dopamine and Acetylcholine Receptors. *The*
892 *Journal of neuroscience : the official journal of the Society for Neuroscience* 37:11166-
893 11180.
- 894 Shin JH, Adrover MF, Wess J, Alvarez VA (2015) Muscarinic regulation of dopamine and
895 glutamate transmission in the nucleus accumbens. *Proceedings of the National Academy*
896 *of Sciences of the United States of America* 112:8124-8129.
- 897 Sulzer D, Cragg SJ, Rice ME (2016) Striatal dopamine neurotransmission: regulation of release
898 and uptake. *Basal ganglia* 6:123-148.
- 899 Surmeier DJ, Ding J, Day M, Wang Z, Shen W (2007) D1 and D2 dopamine-receptor
900 modulation of striatal glutamatergic signaling in striatal medium spiny neurons. *Trends in*
901 *neurosciences* 30:228-235.

- 902 Taber MT, Fibiger HC (1993) Electrical stimulation of the medial prefrontal cortex increases
903 dopamine release in the striatum. *Neuropsychopharmacology* : official publication of the
904 American College of Neuropsychopharmacology 9:271-275.
- 905 Taber MT, Fibiger HC (1994) Cortical regulation of acetylcholine release in rat striatum. *Brain*
906 research 639:354-356.
- 907 Threlfell S, Lalic T, Platt NJ, Jennings KA, Deisseroth K, Cragg SJ (2012) Striatal dopamine
908 release is triggered by synchronized activity in cholinergic interneurons. *Neuron* 75:58-
909 64.
- 910 Threlfell S, Clements MA, Khodai T, Pienaar IS, Exley R, Wess J, Cragg SJ (2010) Striatal
911 muscarinic receptors promote activity dependence of dopamine transmission via distinct
912 receptor subtypes on cholinergic interneurons in ventral versus dorsal striatum. *The*
913 *Journal of neuroscience* : the official journal of the Society for Neuroscience 30:3398-
914 3408.
- 915 Tritsch NX, Sabatini BL (2012) Dopaminergic modulation of synaptic transmission in cortex and
916 striatum. *Neuron* 76:33-50.
- 917 Tritschler L, Kheirbek MA, Dantec YL, Mendez-David I, Guilloux JP, Faye C, Doan J, Pham
918 TH, Hen R, David DJ, Gardier AM (2018) Optogenetic activation of granule cells in the
919 dorsal dentate gyrus enhances dopaminergic neurotransmission in the Nucleus
920 Accumbens. *Neurosci Res* 134:56-60.
- 921 Vidal CJ, Chai MS, Plummer DT (1987) The effect of temperature on the activity of
922 acetylcholinesterase preparations from rat brain. *Neurochem Int* 11:135-141.
- 923 Voorn P, Vanderschuren LJ, Groenewegen HJ, Robbins TW, Pennartz CM (2004) Putting a spin
924 on the dorsal-ventral divide of the striatum. *Trends in neurosciences* 27:468-474.
- 925 Wang L, Shang S, Kang X, Teng S, Zhu F, Liu B, Wu Q, Li M, Liu W, Xu H, Zhou L, Jiao R,
926 Dou H, Zuo P, Zhang X, Zheng L, Wang S, Wang C, Zhou Z (2014) Modulation of
927 dopamine release in the striatum by physiologically relevant levels of nicotine. *Nature*
928 *communications* 5:3925.
- 929 Zhang H, Sulzer D (2004) Frequency-dependent modulation of dopamine release by nicotine.
930 *Nature neuroscience* 7:581-582.
- 931 Zhou FM, Liang Y, Dani JA (2001) Endogenous nicotinic cholinergic activity regulates
932 dopamine release in the striatum. *Nature neuroscience* 4:1224-1229.
- 933 Zhu J, Hexum TD (1992) Characterization of cocaine-sensitive dopamine uptake in PC12 cells.
934 *Neurochem Int* 21:521-526.
- 935

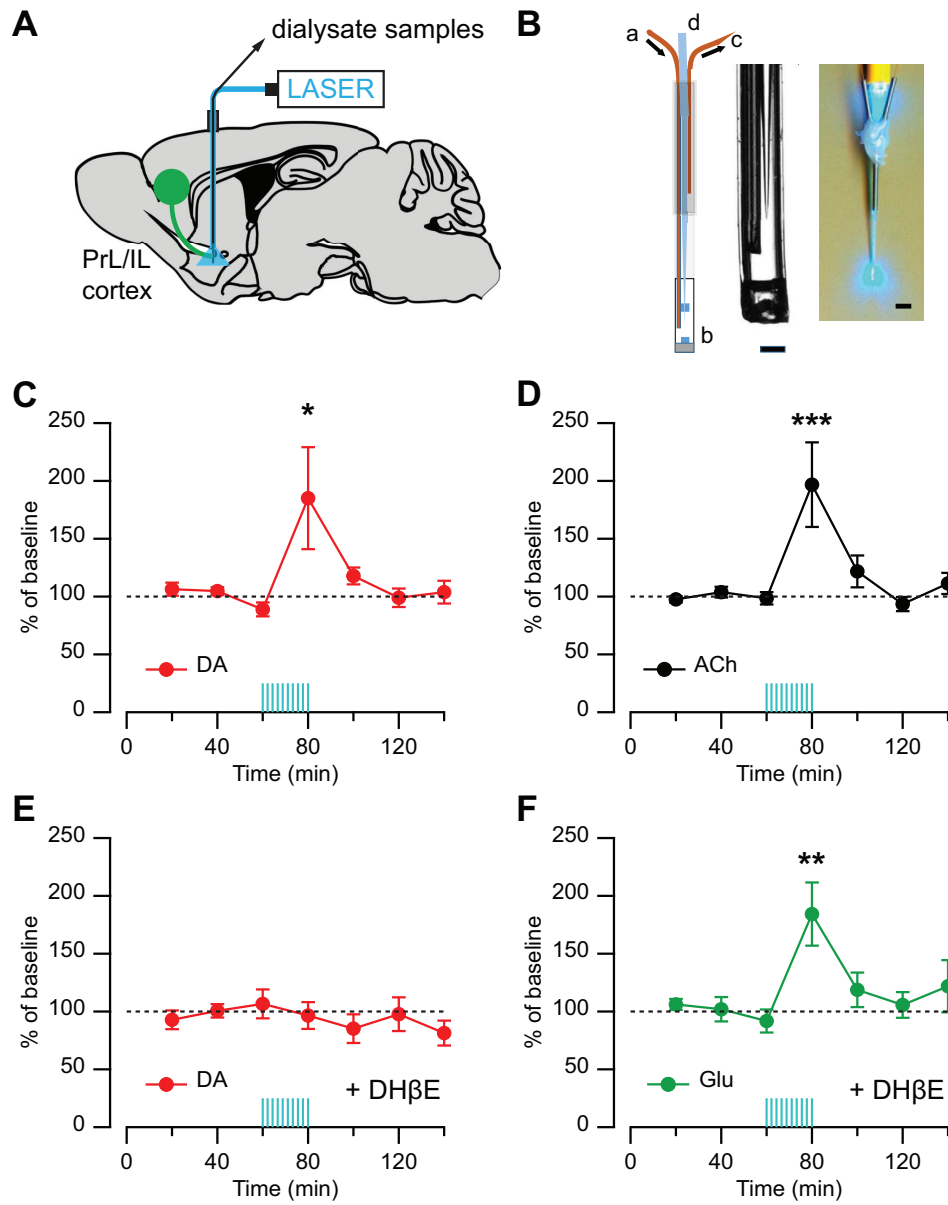


Figure 1 of Adrover et al.

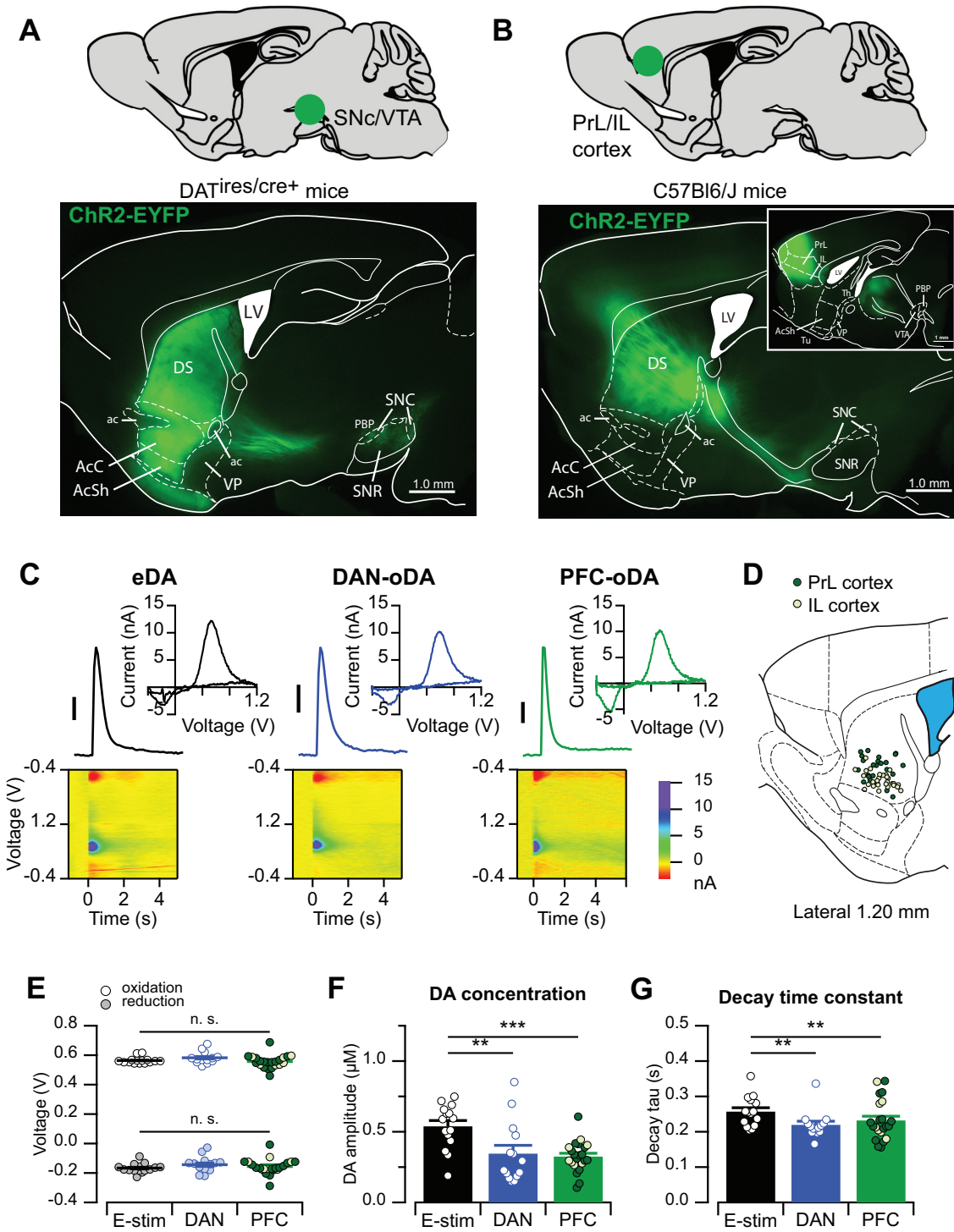


Figure 2 of Adrover et al.

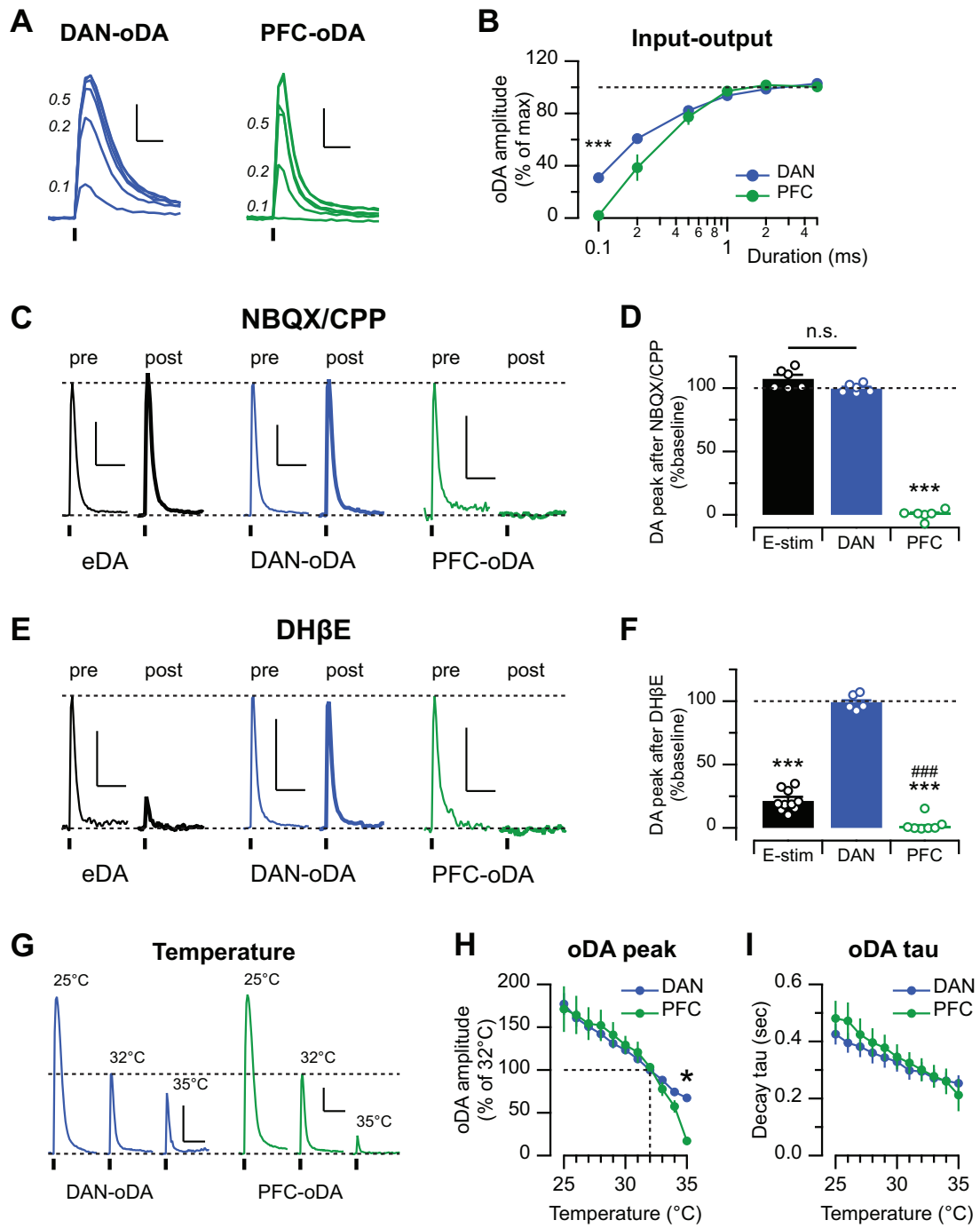


Figure 3 of Adrover et al.

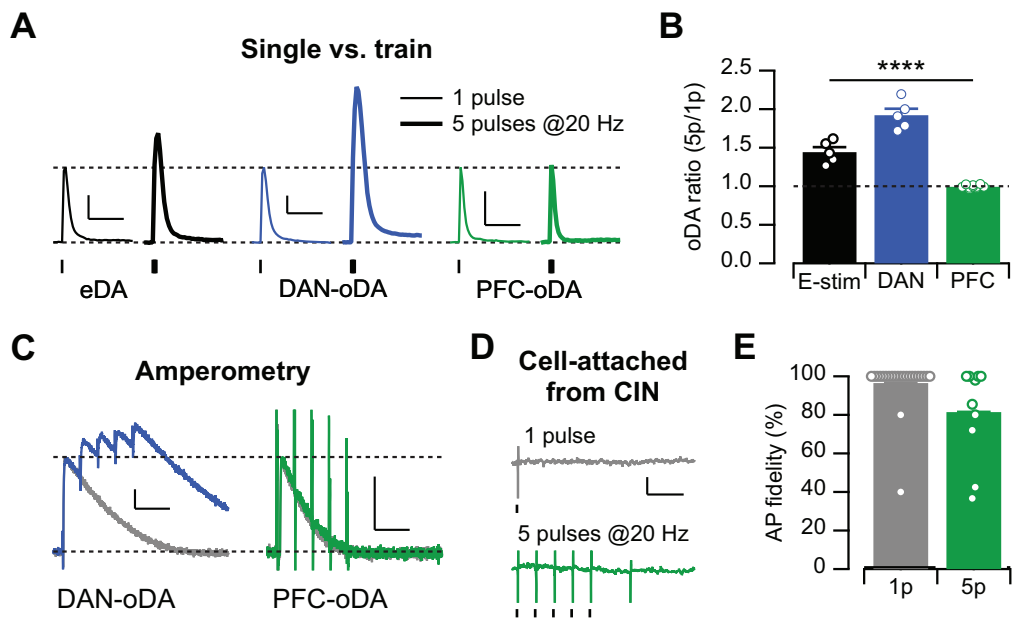


Figure 4 of Adrover et al.

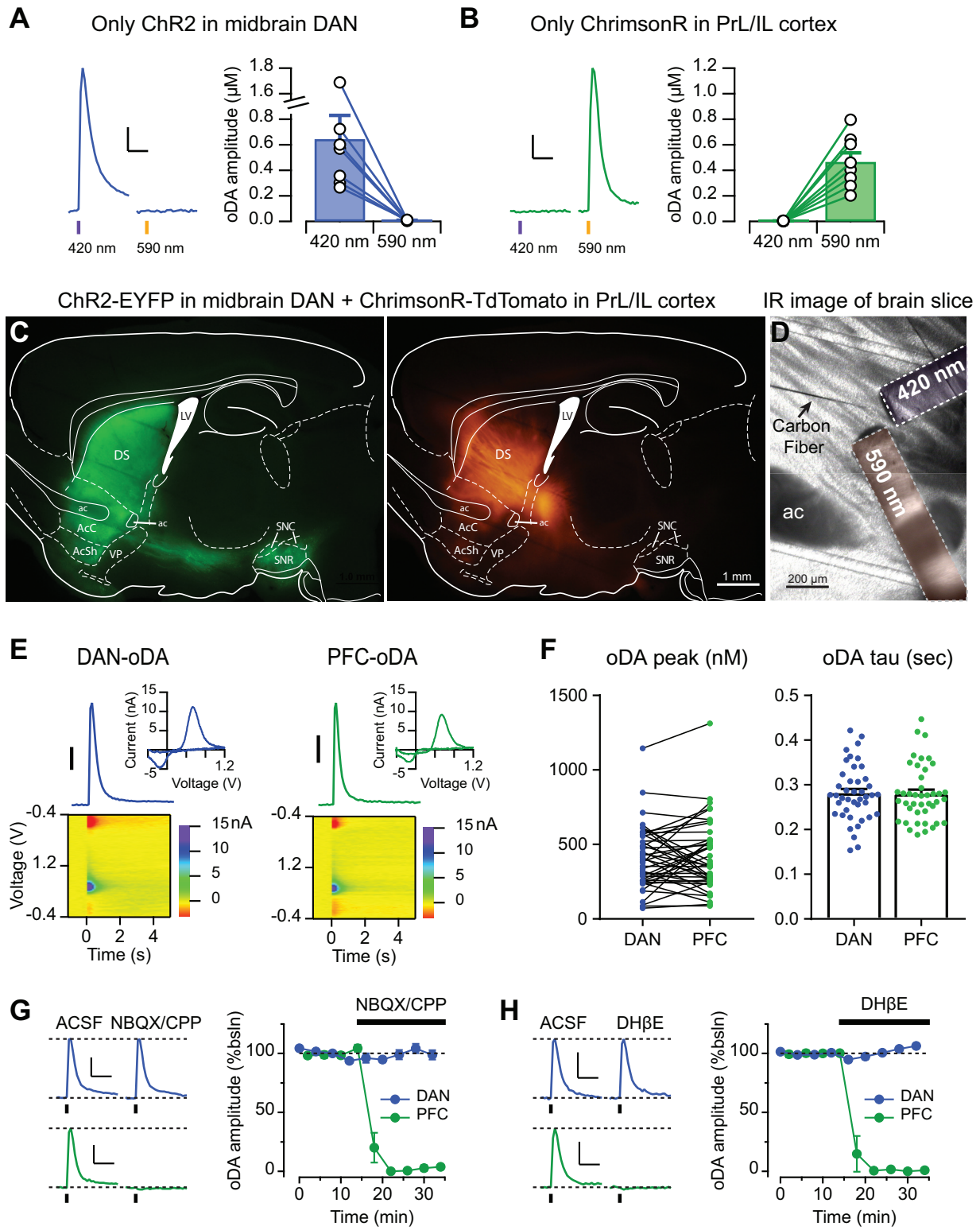


Figure 5 of Adrover et al.

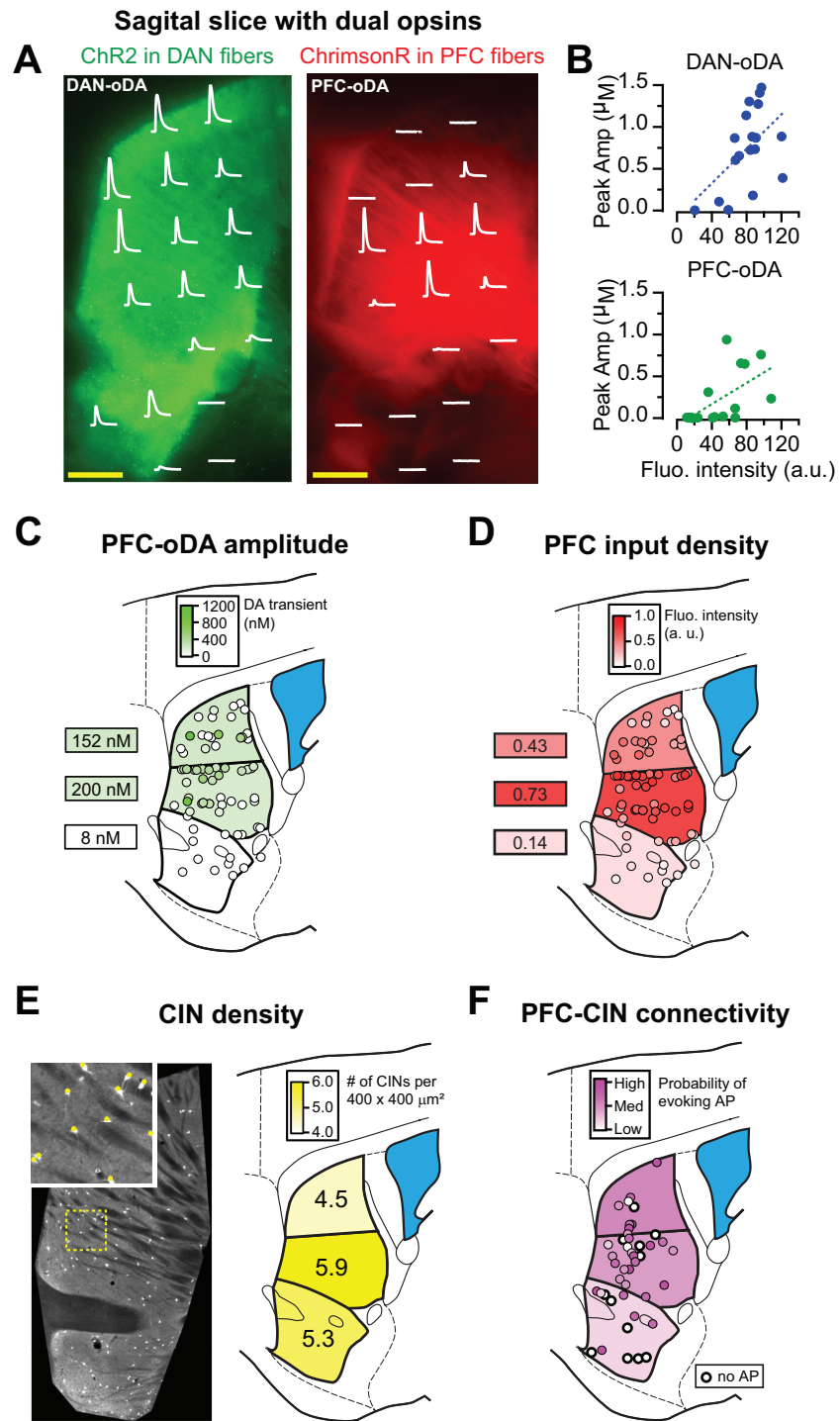


Figure 6 of Adrover et al.